Precision Agriculture (2022) 23:300–318
https://doi.org/10.1007/s11119-021-09838-3

Coffee ripeness monitoring using a UAV-mounted low-cost multispectral camera

Jorge Tadeu Fim Rosas[1] · Francisco de Assis de Carvalho Pinto[2] · Daniel Marçal de Queiroz[2] · Flora Maria de Melo Villar[2] · Domingos Sárvio Magalhães Valente[2] · Rodrigo Nogueira Martins[2]

Accepted: 18 August 2021 / Published online: 26 August 2021
© The Author(s), under exclusive licence to Springer Science+Business Media, LLC, part of Springer Nature 2021

Abstract
Coffee beverage quality is highly correlated with the degree of fruit ripeness. In this sense, monitoring fruit ripeness is of utmost importance for harvest planning and, especially for obtaining high-quality beverages. Currently, this process is carried out through manual counts of unripe fruits, which is laborious and limited to a few plants within the field. This study aimed at evaluating the potential of a low-cost multispectral camera for coffee ripeness monitoring in the *Zona da Mata* region of Minas Gerais State, Brazil. For that, five fields of Arabica coffee with distinct characteristics were evaluated. During the coffee ripeness period, four flights were carried using a Phantom 4 Pro quadcopter equipped with a Mapir Survey 3W camera for imagery acquisition. After that, nine vegetation indices (VIs) were obtained. For the same dates, the percentage of unripe fruits was obtained using an irregular grid in all fields. The data was split into two ripeness classes: suitable for harvest (R) with < 30% of unripe fruits; and not suitable for harvest (U), with > 30% of unripe fruits. Then, a principal component analysis was used to infer the importance of the VIs to discriminate plants with unripe fruits from those with ripe fruits. The first two principal components explained > 75% of the variance in the datasets from all coffee fields. The VIs were able to discriminate the ripeness classes (U and R) in most fields; however, their performance was directly influenced by the crop yield and canopy volume.

Keywords Unmanned aerial vehicle · Remote sensing · Modified camera · Fruit ripeness · *Coffea arabica* L.

Introduction

Currently, the concern of coffee producers is not only limited to crop productivity, but also to factors that add value to the final product that need to be taken into account within the crop production system (Volsi et al., 2019). Coffee is one of the few agricultural products

✉ Jorge Tadeu Fim Rosas
jorge.fimrosas@gmail.com

[1] Department of Soil and Plant Nutrition, University of São Paulo (USP-ESALQ), Piracicaba, Brazil

[2] Department of Agricultural Engineering, Federal University of Viçosa (UFV), Viçosa, Brazil

whose prices are based on qualitative parameters in Brazil, and its value is significantly increased with quality improvement (Guimarães et al., 2019; Paseto & Patino, 2019; Simões et al., 2008).

The quality of coffee beans is affected by several factors, such as altitude, plant nutrition, period of exposure of the crop to solar radiation and presence or absence of diseases, and most importantly, by the fruit ripeness degree at harvest (Fagan et al., 2011; Pimenta et al., 2018; Simões et al., 2008; Varão et al., 2019). Harvesting the crop at inappropriate times affects the sensory quality of the beverages, as well as the bean color uniformity after post-harvest processing. Coffee fruits harvested when still green will produce defective beans with dark shades after being processed, which depreciates the bean quality and makes the beverage bitter (Aparecido et al., 2018). Based on this, due to the importance of the fruit ripeness degree at harvest for the production of higher quality coffees, it is indispensable to monitor the fruits on the plant and thus determine the optimal harvest time.

Currently, coffee ripeness monitoring is carried out through manual counts of unripe and ripe fruits. This method is laborious, time-consuming, and limited to a few plants within the field, which are not fully representative. An alternative to this method would be the use of remote sensing (RS), which enables non-destructive sampling over the entire area of interest. Remote sensing has been increasingly used for monitoring various crops. For the coffee crop, a few studies have been conducted for disease monitoring (Marin et al., 2019) biophysical parameters estimation (Ramirez & Zullo Júnior, 2010), and also for yield estimation (Nogueira et al., 2018). This demonstrates the applicability of this tool for coffee crop monitoring. However, there are some limitations to this type of analysis, which includes the fact that public domain images obtained by orbital platforms have low temporal and spatial resolution, that may compromise monitoring procedures that require fast decision-making.

With the advent of unmanned aerial vehicle (UAVs), the limitations in the acquisition of spectral information at a suitable temporal resolution, and to the cost of high spatial resolution imagery have been overcome (Zhang & Kovacs, 2012). UAVs have been widely used in studies related to crop monitoring, due to their relatively low cost of acquisition, compared to other platforms, and ability to obtain images with a high spatial resolution (~0.01 m) (Lelong et al., 2008). In addition, the technological advances related to the sensors, which are carried on board these aircraft, have enabled the acquisition of images with high spectral resolution.

Multispectral images obtained by UAVs have been used for forage species identification (Lu & He, 2017) estimation of soybean physiological maturity and yield (Yu et al., 2016) nitrogen monitoring and fertilization (Corti et al., 2019; Parreiras et al., 2020) and biophysical parameters estimation (Santos et al., 2020). For fruit ripeness monitoring, UAVs have been used in a few crops, such as tomato (Senthilnath et al., 2016), apple (Valente et al., 2019), and coffee (Furfaro et al., 2007; Herwitz et al., 2004; Johnson et al., 2004). However, even though there are studies that have attempted to monitor the coffee ripeness using UAV images, none of these studies considered the spatial variability of the fruit ripeness within a coffee field, but rather focused on mean differences between fields.

Currently, several multispectral sensors are commercially available. However, these sensors are still costly (~US$ 5000), which makes them inaccessible to small farmers. An alternative to this problem is the use of modified sensors, which can cost ten times less than typical multispectral sensors for agriculture, and are characterized as low-cost sensors (Putra & Soni, 2017). These devices are RGB (red, green, and blue) cameras that are modified to register radiation in the near-infrared band (NIR) (Coburn et al., 2018; Corti et al., 2019). This is possible because these sensors are mostly equipped with CMOS

(complementary metal–oxide–semiconductor) and CCD (charge-coupled device) sensors that are sensitive to the NIR band, and therefore, can be used to obtain information in this range of the electromagnetic spectrum (Nijland et al., 2014).

Despite the apparent potential for using modified RGB cameras to acquire multispectral images, only a few studies have discussed the uncertainties of using these sensors. The acquisition of multispectral images using cameras with a single sensor is a major challenge since CMOS and CCD sensors do not have the same quantum efficiency for the different wavelengths registered by the device (Lulé et al., 2000). Another issue is that the band-pass nano-filter networks used in these sensors are not able to filter 100% of the unwanted radiation (Lebourgeois et al., 2008).

In summary, there is a lack of low-cost systems that can be used to provide faster and more timely measurements of fruit ripeness in coffee for defining the optimal harvest time, which would enable a coffee with superior quality. UAVs are platforms that have the potential of monitoring coffee areas, providing faster and reliable information for defining the ideal harvest time. Therefore, this study aimed at evaluating the potential of a UAV-mounted low-cost multispectral camera for coffee ripeness monitoring in the *Zona da Mata* region of Minas Gerais State, Brazil.

Materials and methods

Study area

The experiment was carried out at the Jatobá farm, municipality of Paula Cândido, in the *Zona da Mata* region of Minas Gerais State, Brazil (Fig. 1). The data collection was performed during the fruit ripeness stage on four dates in April (29th) and May (7, 13, and 27th) 2019.

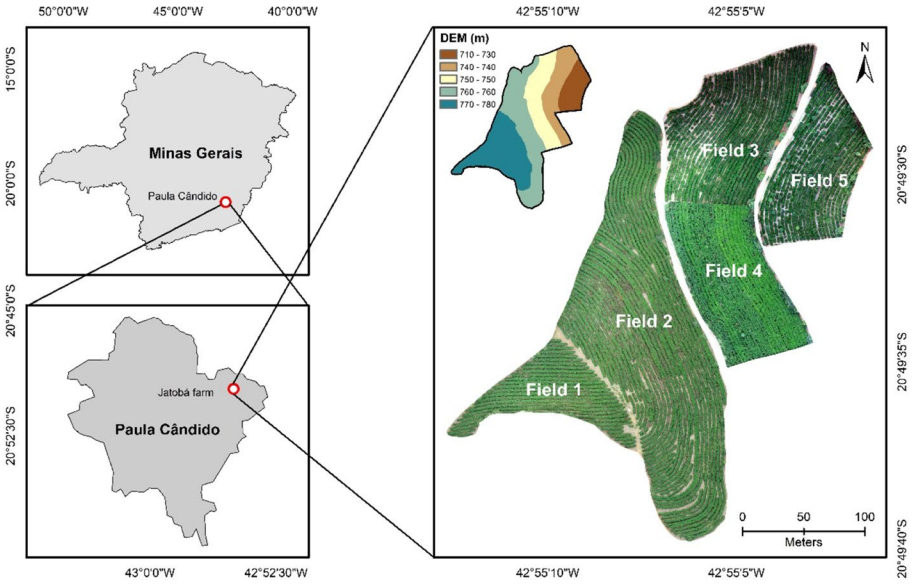

Fig. 1 Study area located in the municipality of Paula Cândido, Minas Gerais State, Brazil

For this study, five fields of Arabica coffee with distinct characteristics were used (Table 1). With the exception of the canopy volume, the remaining data for the characterization of the coffee fields were obtained from the farmer. The canopy volume was calculated using the methodology proposed by Favarin et al. (2002), in which the height and the lower diameter of 25 plants per field were used as input.

UAV platform used to acquire images

The study was conducted using a Phantom 4 Pro quadcopter (DJI Innovations, Shenzhen, China). The flights were planed using the DroneDeploy software (Infatics Inc., San Francisco, California, USA), in which the UAV was set to operate at a speed of 7 m s^{-1} during image acquisition and at an altitude of 60 m above ground level, taking as a reference the highest point of altitude in the study area. The flight plan ensured 70% front overlap and 75% side overlap between the images. Lastly, all flights were carried out between 11:00 and 13:00 h local time under clear sky conditions and on the same days as the manual crop sampling.

All images were obtained using a modified camera, the MAPIR Survey 3W (Peau Productions Inc., San Diego, California, USA). This camera is equipped with a CMOS Sony Exmor R IMX117 sensor, capable of recording images with 12 MP resolution, 24-bit pixel depth in JPEG (Joint Photographic Experts Group) format and 36-bit in the RAW format (format in which the image data are minimally processed). The sensor was originally designed to register the RGB bands. Then, the manufacturer modified it by replacing the filter that prevents the passage of the NIR band, for another that could register only the R–G–NIR (Red, Green, and NIR) bands.

The camera settings were defined on previous field tests and were kept the same for all flights. The condition for choosing these settings was that there were no saturated pixels in any bands of the camera. Thus, the following settings were defined: the shutter aperture speed was fixed at 1/500 s; the ISO sensitivity was set to 100; a 2.8 f-stop; and a focus set up on infinity. The images were acquired in 36-bit RAW format (12 bits per band), which was chosen due to the absence of any type of processing and compression in the images obtained by the sensor.

Table 1 Characteristics of the coffee fields evaluated in the municipality of Paula Cândido, Minas Gerais State, Brazil

Field	Area (ha)	Cultivar	Fruit color	Canopy volume (m^3)	Density (Plants ha^{-1})	Yield[a] (t ha^{-1})
1	0.54	Red Catuai	Red	2.91 ± 0.19	4000	1.20
2	2.1	Red Catuai	Red	1.87 ± 0.14	4000	0.48
3	1.01	MG H 4191	Yellow	0.62 ± 0.04	8000	3.75
4	0.77	Red Burbon	Red	0.70 ± 0.06	13 333	2.49
5	0.65	Icatu	Red	1.77 ± 0.10	2222	2.22

t ton

[a]Average crop yield in the 2018–2019 season

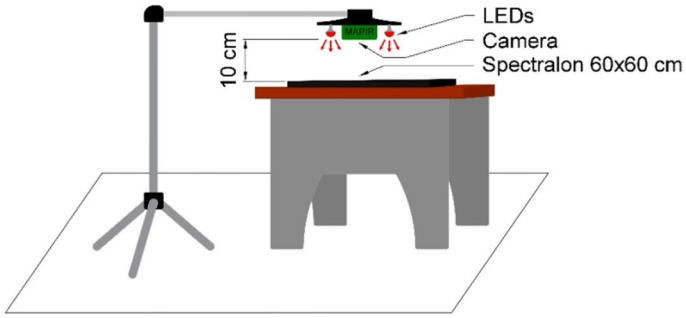

Fig. 2 Structure mounted to study the radiometric quality of the Survey 3W bands

Table 2 Characterization of the LEDs used to study the radiometric quality of the Survey 3W bands

LED	Band (nm)	Power (W)	Light intensity (lx)
Blue	450–490	3	3200
Green	530–590	3	15 000
Yellow	600–635	3	5500
Red	645–685	3	7200
NIR	830–885	3	16 700

Assessment of image quality

In order to evaluate the radiometric quality of the Survey 3W bands, an experiment using monochromatic light-emitting diodes (LEDs) was conducted in laboratory (Fig. 2). For this, five monochromatic lights were used in the wavelengths of blue, green, yellow, red and NIR. A luxmeter was used to determine the light intensity of each LED, and a portable spectroradiometer ASD Handheld 2 (Analytical Spectral Devices, Inc., Boulder, Colorado, USA) was used to determine their emitting range. The characteristics of the LEDs are presented in Table 2.

The LEDs were used to illuminate a spectralon plate that reflected 99% of the incident radiation. Then, five images of this plate were obtained under each of the evaluated illuminations. The camera settings for this experiment were the same as those defined to obtain the field images. After image acquisition, the average value of the digital numbers (DNs) in each band under the different illuminations was calculated.

Another test to evaluate the radiometric quality of the images obtained by the Survey 3W was the analysis of the signal-to-noise ratio (SNR). For this, the ratio between the mean and standard deviation of a homogeneous surface contained in the scene was used to estimate the SNR (Eq. 1) (Hruska et al., 2012; Lu & He, 2017).

$$SNR = 20log_{10}\left(\frac{Dpm}{Np}\right) \quad (1)$$

where *SNR*, signal-to-noise ratio expressed in decibels; *Dpm*, mean digital number on the homogeneous surface; and *Np*, standard deviation of the digital numbers on the homogeneous surface.

In total, six homogeneous surfaces were used: the roof of a building (2.00 × 1.80 m), a region of exposed soil (2.00 × 2.00 m), a region in a lake (2.00 × 2.00 m), a black target (0.50 × 0.50 m), a white target (0.50 × 0.50 m), and a red target (0.50 × 0.50 m). All targets were present in the study area.

Image mosaicking and orthorectification

A total of four orthomosaics with a spatial resolution of approximately 0.03 m were generated using 90 images collected for each flight. For this, the OpenDroneMap (ODM), version 0.4.1 ("GitHub-OpenDroneMap/ODM", n.d.) was used through its web interface, the WebODM application ("GitHub-OpenDroneMap/WebODM", n.d.). The WebODM consists of a set of tools designed to process and analyze UAV imagery.

The orthomosaic creation consisted of five steps: (1) extraction of image metadata, which contained information about the sensor and its geographic location; (2) image alignment, in which the position of each image was calculated, and this position was used for precise orientation of individual photos and the generation of a 3D point cloud; (3) densification of the 3D point cloud; (4) digital surface model (DSM) creation; and (5) lastly, the orthomosaic creation using the DSM.

After this, the orthomosaics were geometrically corrected using the software QGIS, version 2.18 (QGIS Development Team, 2016) and the information of the six ground control points (GCPs) coordinates. These GCPs were added in the study area on each flight and, georeferenced using a Trimble ProXT GNSS (Global Navigation Satellite System) topographic receiver (Trimble Inc., United States).

Radiometric correction of images

The coffee ripeness monitoring is a temporal study; consequently, in order to monitor the temporal changes of fruit ripeness throughout the UAV flights, the relative radiometric normalization between the images obtained on different dates was necessary. This correction was performed using the linear Eqs. (2) and (3) proposed by Hall et al. (1991) and adapted by Yu et al. (2016) for UAV imagery processing.

$$Black_{T1,k} = akBlack_{T2,k} + bk \tag{2}$$

$$White_{T1,k} = akWhite_{T2,k} + bk \tag{3}$$

where $Black_{T1,k}$ and $Black_{T2,k}$, are the DNs of the reference dark objects in the k band of images recorded at times T1 and T2; $White_{T1,k}$ and $White_{T2,k}$, are the DNs of the reference light objects in the k band of images recorded at times T1 and T2; and ak, is the slope or gain, and bk is interception or displacement, defined with the resolution of the system of linear equations.

The reference DNs were obtained from targets made of plywood and painted with white (light target) and matte black paint (dark target). These targets were placed in the study area in all flights. The images obtained on April 29 were used as the reference (T1), and the images on the other dates were normalized based on the reference.

After correcting all orthomosaics, their DNs were converted into reflectance values using the vicarious calibration (Del Pozo et al., 2014; Rosas et al., 2020) and four reflectance targets made of plywood and painted with matte paint in four shades of gray. These

targets had dimensions of 0.50 × 0.50 m and were also kept in the study area on all flight dates. Linear regression models were fitted for each band from all flight dates using the average DN values of each target and their laboratory reflectance (Fig. 3). The reflectance of the calibration targets was determined in the laboratory using the ASD HandHeld 2 spectroradiometer, which operates in the wavelength range from 325 to 1075 nm, with an accuracy of ± 1 nm.

Extraction of the spectral variables

The spectral variables consisted of nine vegetation indices (VIs), obtained using the QGIS software. The following VIs were calculated: Coffee Ripeness Index (CRI), Green Normalized Difference Vegetation Index (GNDVI), Modified Chlorophyll Absorption in Reflectance Index 1 (MCARI1), Modified Triangular Vegetation Index 1 (MTVI1), Normalized Difference Vegetation Index (NDVI), Normalized Green–Red Difference Index (NGRDI),

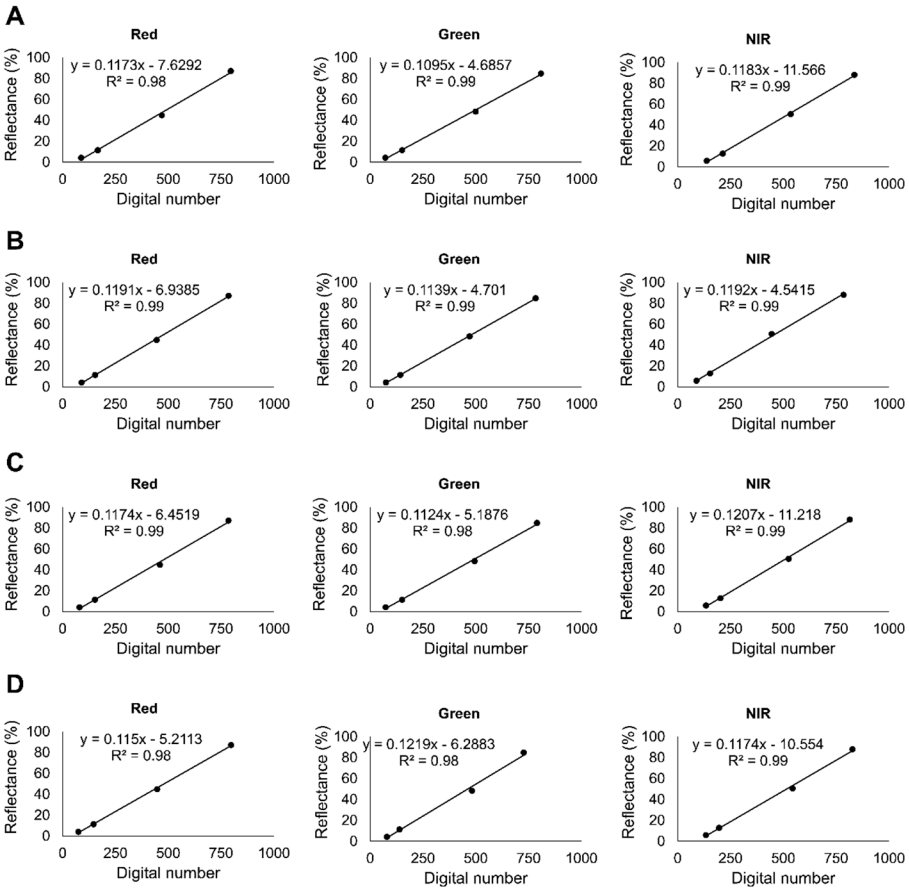

Fig. 3 Linear regression models fitted for the radiometric correction of the three bands of the Survey 3W camera **A** on the first, **B** second, **C** third and **D** fourth flight

Ratio Vegetation Index (RVI), Normalized Ratio Vegetation Index (NRVI), and Simple Ratio (SR) (see Table 3 for formulae and references).

The criteria for selecting the VIs were that the existing bands obtained by the Survey 3W camera could be used for their calculations. The CRI was included because it was created specifically for monitoring coffee ripeness (Nogueira Martins et al., 2021). In addition, all VIs have been shown to be well correlated with either the plant pigments (e.g., chlorophyll, anthocyanins) or with the plant nutritional status. After calculating the VIs, polygonal masks covering the plant canopy were manually created on each sampling point, and the average values of the indices were obtained.

Coffee fruit ripeness monitoring

For field sampling, an irregular grid with 20 sampling points per hectare was defined on each measurement date (Fig. 4). For field 2, only 10 points per hectare were collected due to its lower fruit load. Each sampling point consisted of three plants located side by side in the same row. Four plagiotropic branches, one in each plant quadrant, were randomly chosen in the middle third of each plant. The unripe fruits and the total number of fruits on the branches were counted. From the results obtained in the manual counts, the average percentage of unripe fruits was calculated for each sampling point. Then, the sampled plants were divided into two classes of ripening: suitable for harvest (R), in which the percentage of unripe fruits $< 30\%$, and not suitable for harvest (G), with a percentage of unripe fruits $\geq 30\%$. These plants were georeferenced to obtain the subsequent spectral variables.

Statistical analysis

First, the percentage of unripe fruits and the VIs were submitted to a Pearson's correlation analysis to investigate the existence of a linear association between these variables. Second, an analysis of variance (ANOVA) was carried out to verify whether the VIs could be used to discriminate plants suitable for harvest (R) from those not-suitable for harvest (G). Lastly, a principal component analysis (PCA) was performed on each field to identify the VIs with the greatest importance for coffee ripeness monitoring. The PCA was also used to

Table 3 Vegetation indices used for the coffee fruit ripeness monitoring

Index	Equation	References
CRI	$\left(\mathrm{R}/\mathrm{R}_{\mathrm{target}}\right)100$	Nogueira Martins et al. (2021)
GNDVI	$\frac{\mathrm{NIR}-\mathrm{G}}{\mathrm{NIR}+\mathrm{G}}$	Gitelson et al. (1996)
MCARI1	$1.2[2.5(\mathrm{NIR}-\mathrm{R})-1.3(\mathrm{NIR}-\mathrm{G})]$	Haboudane et al. (2004)
MTVI1	$1.2[1.2(\mathrm{NIR}-\mathrm{G})-2.5(\mathrm{R}-\mathrm{G})]$	Haboudane et al. (2004)
NDVI	$\frac{\mathrm{NIR}-\mathrm{R}}{\mathrm{NIR}+\mathrm{R}}$	Rouse et al. (1973)
NGRDI	$\frac{\mathrm{G}-\mathrm{R}}{\mathrm{G}+\mathrm{R}}$	Tucker (1979)
RVI	$\frac{\mathrm{R}}{\mathrm{NIR}}$	Jordan (1969)
NRVI	$\frac{\mathrm{RVI}-1}{\mathrm{RVI}+1}$	Baret and Guyot (1991)
SR	$\frac{\mathrm{NIR}}{\mathrm{R}}$	Jordan (1969)

NIR near infrared, *R* red, *G* green, R_{Target} average reflectance value of the red target in the red band

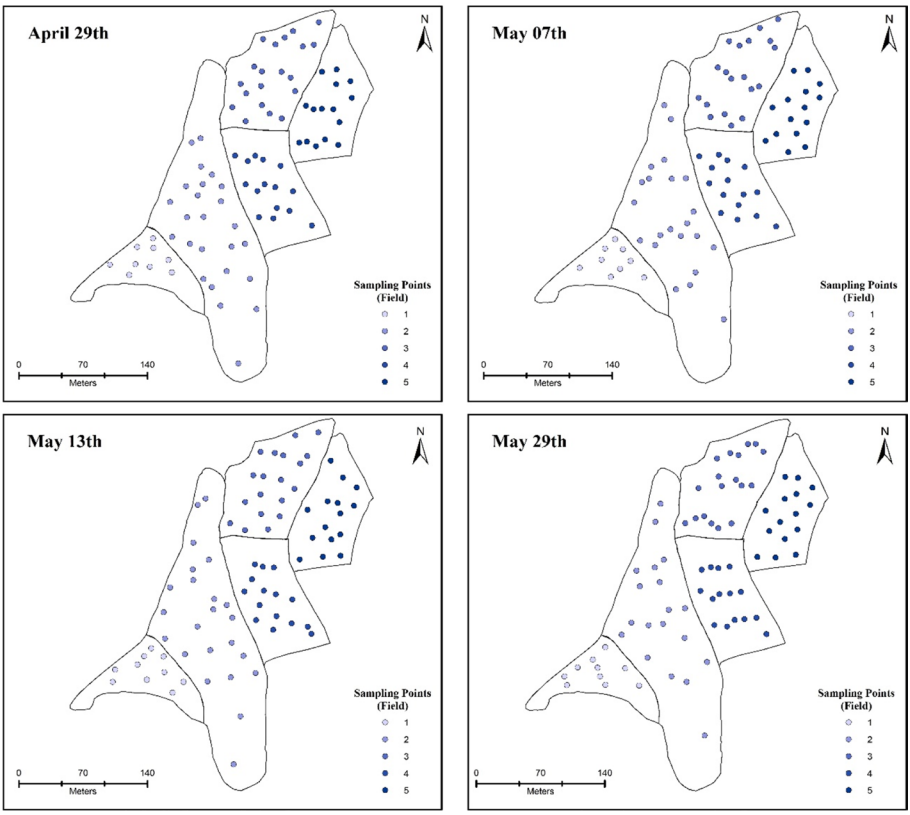

Fig. 4 Spatial distribution of the sampling points used for field measurements of the coffee ripeness

verify the possibility of grouping plants with unripe fruits from those with ripe fruits. All statistical analyses were carried out using the R software (R Core Team, 2019).

Results

Laboratory experiment for image quality assessment

Laboratory pre-tests showed that there was an overlap between the spectral bands of the camera used (Fig. 5). Band 1 (red) was sensitive to all illuminations tested, except for green. Furthermore, the most critical point was observed for the NIR LED that showed an average DN value of 1862.82, which corresponded to 86.6% of the average DN recorded in the NIR band under the same circumstance. On the other hand, band 2 (green) showed the least overlapping with the other bands, presenting only a slight sensitivity to the blue, yellow and NIR LEDs. Band 3 (NIR) was also sensitive to the blue, yellow and red LEDs, especially the red one, in which the average DN value was 377.86, which represented 24.58% of the average DN value in the red band. In summary, the red band presented the highest sensitivity to wavelengths outside the expected range.

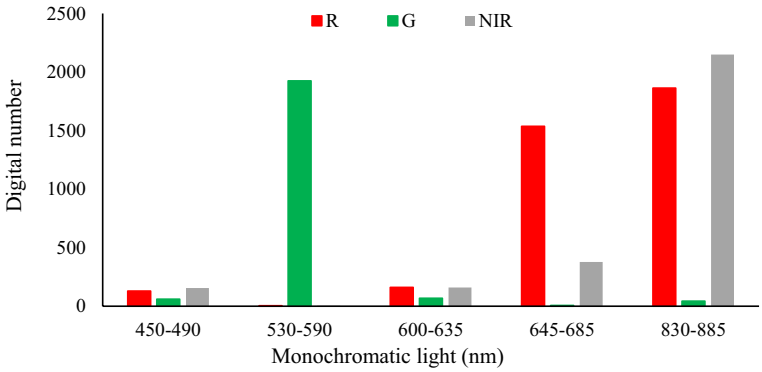

Fig. 5 Sensitivity of the MAPIR Survey 3W bands to five different monochromatic lights

The high sensitivity of the red band to the NIR band becomes a source of error in measurements of radiation emitted by surfaces in field experiments, especially in studies related to vegetation, in which the NIR reflectance is much higher than in the red band. The fact that the red band also recorded radiation from the NIR band led its DN values to be higher than those presented by the green band in situations where the opposite was expected, such as in coffee plants, which present high vegetative vigor (Fig. 6).

The signal-to-noise ratio analysis showed that all three bands presented an SNR above 20 dB for all surfaces (Table 4). In general, the NIR band showed the lowest SNR, with the absolute lowest SNR value observed in the NIR band with the white target, demonstrating that this channel was noisier than the others. Conversely, the highest SNR was obtained in the red band (28.85 dB) with the red target.

Field monitoring of coffee ripeness

Results of the linear correlations between the VIs and the percentage of unripe fruits are presented in Table 5. There were changes in the crop's spectral response as the coffee

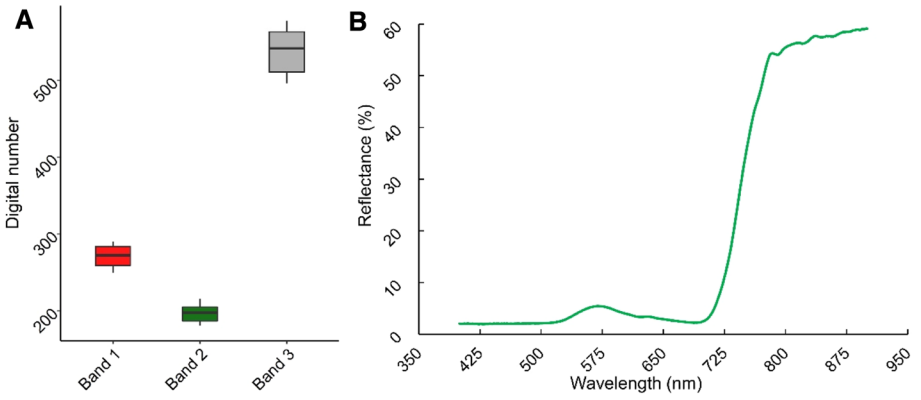

Fig. 6 Spectral response of coffee plants with high vegetative vigor. **A** boxplot of average values of the digital numbers obtained in nine coffee plants in the red (1), green (2) and NIR (3) bands: **B** average spectral signature of nine coffee plants obtained with the spectroradiometer in the field (Color figure online)

Table 4 Signal-to-noise ratio of the Survey 3W bands on six homogeneous surfaces (HS) expressed in decibels (dB)

Band	HS1	HS2	HS3	HS4	HS5	HS6
Red	26.3	27.2	24.5	21.9	21.7	28.9
Green	26.6	28.3	26.9	25.2	23.4	28.2
NIR	27.2	27.1	23.6	23.4	20.5	25.8

HS1, roof; HS2, region of exposed soil; HS3, region in a lake; HS4, black target; HS5, white target; HS6, red target

Table 5 Pearson's linear correlation analysis between the percentage of unripe fruits and the vegetation indices

	CRI	GNDVI	MCARI1	MTVI1	NDVI	NGRDI	NRVI	RVI	SR
Field 1									
Unripe fruits (%)	− 0.295	0.445*	0.165	0.116	0.441*	− 0.310	0.459*	− 0.460*	0.305
Field 2									
Unripe fruits (%)	− 0.340*	0.134	0.113	0.120	0.179	− 0.045	0.098	− 0.166	0.195
Field 3									
Unripe fruits (%)	− 0.725*	0.601*	0.603*	0.601*	0.612*	− 0.385*	0.521*	− 0.600*	0.628*
Field 4									
Unripe fruits (%)	− 0.543*	− 0.140	0.381*	0.374*	0.211	0.204	0.258*	− 0.219	0.190
Field 5									
Unripe fruits (%)	− 0.389*	0.256*	0.461*	0.459*	0.305*	− 0.053	0.261*	− 0.291*	0.322*

*Significant at 5% probability level ($p < 0.05$)

ripeness progressed in the five fields studied. For field 1, the vegetation indices GNDVI, NDVI, and NRVI showed a positive correlation, while the RVI showed a negative correlation. Differently, in field 2, only the CRI showed a significant correlation with the percentage of unripe fruits. Overall, fields 3 and 5 presented higher spectral alterations during the fruit ripeness stage. In Field 3, all VIs were correlated with the percentage of unripe fruits, and for field 5 only the NGRDI showed no significant correlation. Lastly, for field 4, only the CRI, MCARI1, MTVI1, and NRVI presented significant correlations.

In order to assess the potential of the VIs to discriminate the fruit ripeness classes (U and R), an ANOVA was performed. The results are presented in Table 6. For field 1, none of the VIs presented significant differences ($p < 0.05$) among the ripeness classes. In field 2, only the CRI was capable of discriminating the ripeness classes. Conversely, for field 3, all VIs were capable of discriminating plants suitable for harvest from those not suitable for harvest. The VIs CRI, MCARI1, and MTVI1 were the most sensitive to the spectral changes caused by the fruit ripeness since they presented significant differences in the majority of the fields.

In addition, the fields in which the VIs showed significant differences among the ripeness classes were also the ones with the highest yield, especially fields 3 and 4, whose

Table 6 Analysis of variance of the vegetation indices average values for the coffee ripeness classes (U and R) in each field

VI	Field 1			Field 2			Field 3		
	U ± SE	R ± SE	p-value	U ± SE	R ± SE	p-value	U ± SE	R ± SE	p-value
CRI	11.388 ± 0.471	11.345 ± 0.778	0.964	11.372 ± 0.208	12.430 ± 0.512	0.028*	10.042 ± 0.112	11.905 ± 0.226	0.000***
GNDVI	0.467 ± 0.002	0.457 ± 0.008	0.119	0.456 ± 0.001	0.453 ± 0.003	0.318	0.461 ± 0.002	0.441 ± 0.004	0.000***
MCARI1	0.076 ± 0.005	0.070 ± 0.007	0.554	0.090 ± 0.002	0.082 ± 0.005	0.166	0.088 ± 0.002	0.058 ± 0.004	0.000***
MTVI1	0.041 ± 0.003	0.039 ± 0.004	0.795	0.049 ± 0.001	0.045 ± 0.003	0.170	0.046 ± 0.001	0.030 ± 0.002	0.000***
NDVI	0.324 ± 0.001	0.323 ± 0.001	0.605	0.322 ± 0.001	0.320 ± 0.002	0.307	0.320 ± 0.001	0.304 ± 0.004	0.000***
NGRDI	− 0.168 ± 0.002	− 0.160 ± 0.008	0.157	− 0.158 ± 0.001	− 0.156 ± 0.002	0.507	− 0.165 ± 0.001	− 0.158 ± 0.002	0.002**
NRVI	− 0.337 ± 0.001	− 0.338 ± 0.001	0.397	− 0.336 ± 0.001	− 0.338 ± 0.002	0.371	− 0.336 ± 0.001	− 0.346 ± 0.002	0.000***
RVI	0.511 ± 0.002	0.513 ± 0.002	0.524	0.513 ± 0.001	0.516 ± 0.002	0.353	0.516 ± 0.002	0.535 ± 0.005	0.000***
SR	1.965 ± 0.006	1.968 ± 0.008	0.791	1.956 ± 0.004	1.946 ± 0.007	0.252	1.948 ± 0.005	1.884 ± 0.014	0.000***
N	29	9		68	20		51	24	

	Field 4			Field 5		
	U ± SE	R ± SE	p-value	U ± SE	R ± SE	p-value
CRI	11.037 ± 0.280	14.441 ± 0.273	0.000***	11.162 ± 0.258	13.781 ± 0.742	0.000***
GNDVI	0.460 ± 0.002	0.466 ± 0.003	0.000***	0.448 ± 0.002	0.446 ± 0.004	0.631
MCARI1	0.105 ± 0.003	0.088 ± 0.006	0.004**	0.087 ± 0.002	0.064 ± 0.004	0.000***
MTVI1	0.058 ± 0.002	0.047 ± 0.003	0.002**	0.047 ± 0.001	0.034 ± 0.002	0.000***
NDVI	0.328 ± 0.0004	0.326 ± 0.001	0.033*	0.314 ± 0.002	0.310 ± 0.003	0.296
NGRDI	− 0.156 ± 0.002	− 0.166 ± 0.003	0.017*	− 0.157 ± 0.002	− 0.159 ± 0.002	0.615
NRVI	0.334 ± 0.001	0.337 ± 0.001	0.019*	− 0.338 ± 0.002	− 0.344 ± 0.002	0.115
RVI	0.507 ± 0.0004	0.509 ± 0.001	0.028*	0.524 ± 0.002	0.528 ± 0.004	0.338
SR	1.977 ± 0.002	1.969 ± 0.005	0.053	1.922 ± 0.007	1.904 ± 0.013	0.242
N	42	18		45	15	

R: Average values of the vegetation indices from plants suitable to harvest; U: Average values of the vegetation indices from plant not-suitable for harvest; SE: standard error

***Significant at 0.1% probability level

**Significant at 1% probability level

*Significant at 5% probability level

average yield values were 3.75 and 2.49 t ha^{-1}. These fields were also those with the highest plant density and lowest canopy volume. On the other hand, fields 1 and 2, in which the VIs had practically no significant differences among the ripeness classes presented the lowest yields (1.20 and 0.48 t ha^{-1}), and also the highest canopy volumes (Table 1).

Results of the PCA showed that the first two components were able to explain more than 70% of the variance in the dataset from all coffee fields. Figure 6 presents the biplots between PC1 and PC2 for the five fields and also the vectors representing the VIs. In general, there was a common pattern in the importance of the variables for all fields in these two PCs. For PC1, the most important VIs were GNDVI, NDVI, RVI, and SR, while, in PC2 the MTVI1, MCARI1, and NGRDI were the most representative, except for fields 3 and 4, where only the first two VIs showed greater contributions.

The PCA biplots reinforce the difficulty of discriminating plants with ripe fruits from those with unripe fruits in fields 1 and 2 (Fig. 7A and B). Differently, for fields 3, 4 and 5 (Fig. 7C–E), it was possible to observe a pattern of grouping into two groups, in which the yellow triangles represent plants with unripe fruits, while the blue dots represent those with ripe fruits. Specifically, for fields 3 and 4, the discrimination between the two groups was observed more clearly.

Discussion

The existence of an overlapping response between spectral bands is common in modified cameras (Coburn et al., 2018; Corti et al., 2019; Logie & Coburn, 2018). The use of filters that prevent the NIR passage in RGB cameras before the Bayer matrix nano-filter networks, is aimed at preventing pollution in the visible bands. The need for a NIR filter to acquire information in the visible region is due to two factors: (1) the silicon diode constituting the CMOs is sensitive to the NIR band; and (2) the band-pass filters used in the Bayer matrix are not always able to filter 100% of the NIR (Lebourgeois et al., 2008). For the Survey 3W, the NIR blocking filter was removed by the manufacturer so that the NIR band could be recorded instead of the blue band; however, this modification affected the red band, which showed sensitivity to the NIR wavelength.

In addition, another fact that should be considered when intending to use a single sensor for the acquisition of multispectral images is the sensitivity of the CMOs, which is not the same for all wavelengths (Lulé et al., 2000). In modified cameras, such as the one used in the present study, the same shutter aperture and ISO settings were kept for all bands as the same sensor was used to obtain the different bands. Studies conducted by Lebourgeois et al. (2008) overcame this limitation by using an RGB camera without modification and another modified to obtain the NIR, and thus obtain multispectral images.

In this sense, knowing the sensitivity of the CMOs used permits the exposure time and the ISO of the sensor to be adjusted to overcome this problem. According to Rabatel et al. (2014), these limitations that are related to sensor sensitivity can also be overcome through band simulation by orthogonal projection, if the sensor sensitivity curve is known (but this is not always an easy information to obtain). Thus, better results are achieved when only one sensor is used. However, this method worsens the signal-to-noise ratio of the images obtained (Rabatel et al., 2014).

The presence of noise generated by NIR radiation in the red band led to an overestimation of the DNs values from this band, whose DN values were the sum of the red radiation and part of the NIR radiation reflected by the surfaces. Results presented by Lu and He

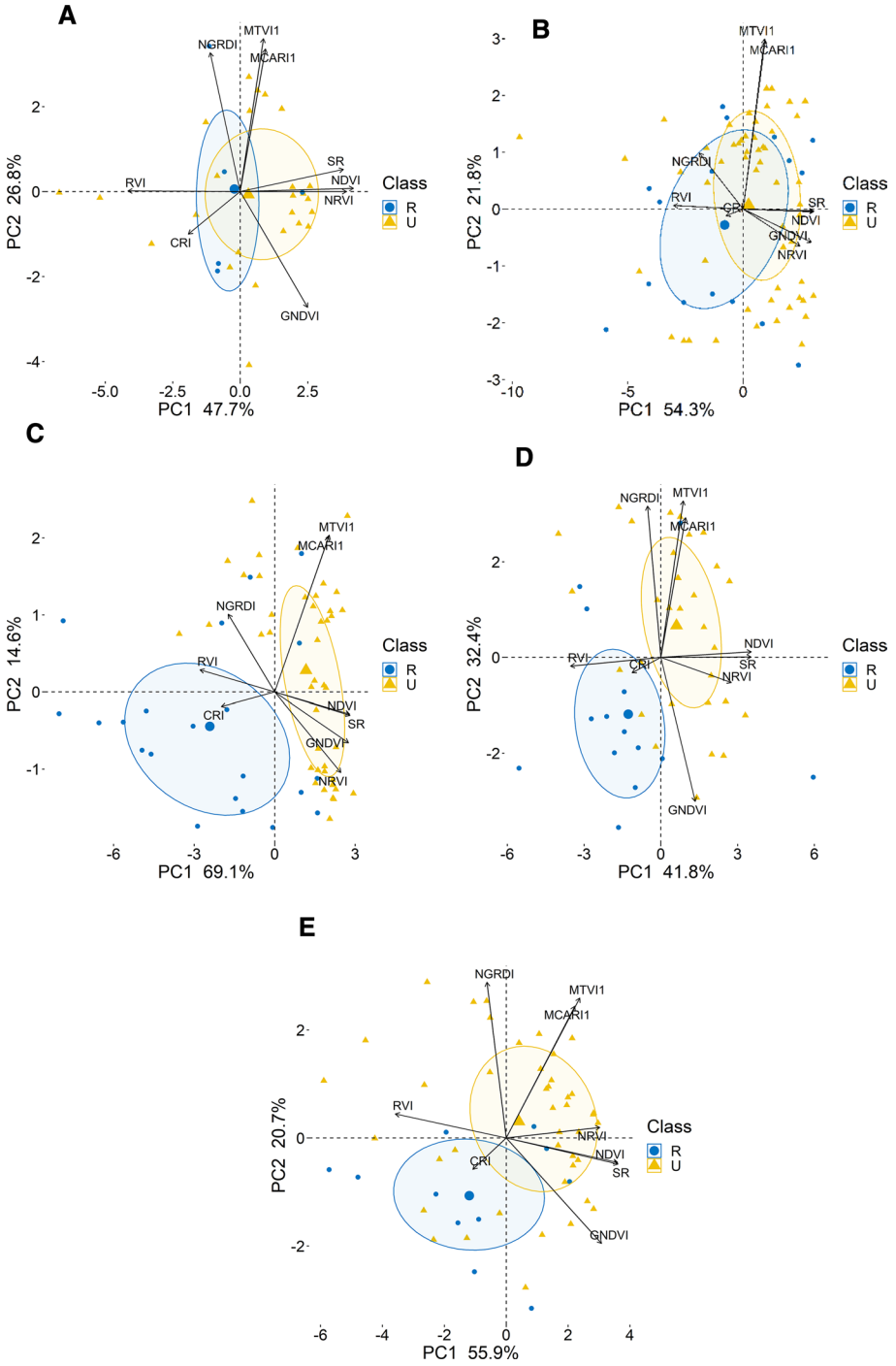

Fig. 7 Results of the principal components analysis (PCA) for the vegetation indices from the plants sampled in the coffee fields. Ellipses drawn following *t* distribution with 95% confidence interval. Field 1 (**A**), Field 2 (**B**), Field 3 (**C**), Field 4 (**D**), Field 5 (**E**) (Color figure online)

(2017) resemble the spectral characteristics found in this study, in which the DN values in the blue band were higher than those in the green band when images of vegetation were obtained using a modified camera. The relationship between the raw digital number of the image and the reflectance of the surfaces assumed a linear behavior, as demonstrated in previous studies (Iqbal et al., 2018; Wang & Myint, 2015). Therefore, low raw DNs should be expected on surfaces with low reflectance; if this does not occur, high errors will be generated in the radiometric calibration of these images.

SNR is an important parameter for the quality assessment of multispectral images. Low values of SNR indicate noisy images, with pixel values that do not accurately describe reality. Images with higher noise lead to serious errors when working with quantitative characteristics. The SNR found in the present study was higher than 14 dB, a value that was previously considered acceptable for modified sensors (Lu & He, 2017).

The spectral response of the coffee plants varied among the five fields as the fruit ripeness progressed throughout the experiment. The crop yield proved to be an important variable when the intent was to monitor the coffee ripeness. The fields with the highest yield were the ones whose spectral characteristics were most influenced. The last stage of fruit formation requires large amounts of nutrients, which tend to be translocated from the leaves to the fruits (Laviola et al., 2009). Furthermore, plants with higher yield tend to translocate higher amounts of nutrients than those with a lower yield, and this may even cause deficiency of nutrients with accentuated mobility in plant tissues, such as macronutrients (Amaral et al., 2001; Laviola et al., 2009). The physiological translocations of nutrients from the leaves to the fruits can alter the spectral signature of the plant, which makes it possible to infer the fruit ripeness degree.

On the other hand, the interaction between crop yield and canopy volume can also be an important parameter for crop monitoring studies. Fields 3 and 4, besides showing higher yield, also presented lower canopy volumes. This combination resulted in greater amounts of coffee fruits exposed in the plant canopy when the UAV flights were carried out. During the ripeness stage, the fruit color changes from green to red or yellow, and this new color is expected to cause noticeable changes in the plant spectra. Thus, the higher crop yield will result in a greater spectral change. An opposite effect was observed in field 2, which presented the lowest yield. This resulted in the absence of significant correlation, and a lack of differences among the ripeness classes for the majority of the VIs. This lower fruit load was caused by the biennial yield effect, in which the crop presents high and low yield values in alternated years (Bernardes et al., 2012).

The VIs CRI, MCARI1, and MTVI1 showed the greatest sensitivity to detect the spectral changes of fruit ripeness as they were capable of discriminating plants with unripe and ripe fruits in the majority of the coffee fields (Table 6). In Fig. 8, there is a representation of the CRI, MCARI1, and MTVI1 for the two ripeness classes. In this example, the differences among classes can be detected at the pixel level.

As in the results presented by Nogueira Martins et al. (2021), the CRI showed great potential to monitor the coffee ripeness as the highest correlations with the percentage of unripe fruits were obtained using this VI in most fields. The CRI quantifies the proportion of red on the coffee canopy. Besides this, as the fruit ripening progresses, the proportion of red increases, and the CRI is able to detect this increase (Nogueira Martins et al., 2021).

On the other hand, the MCARI1 and MTVI1 are sensitive to chlorophyll variations in plant tissues as reported in previous studies (Huang et al., 2015; Sonobe & Wang, 2017; Vincini et al., 2007). Based on this, the changes presented by these VIs during the fruit ripeness stage might be related to the reduction in leaf nitrogen content at this phenological stage, in which the synthesis of antioxidant compounds in the fruits leads to higher

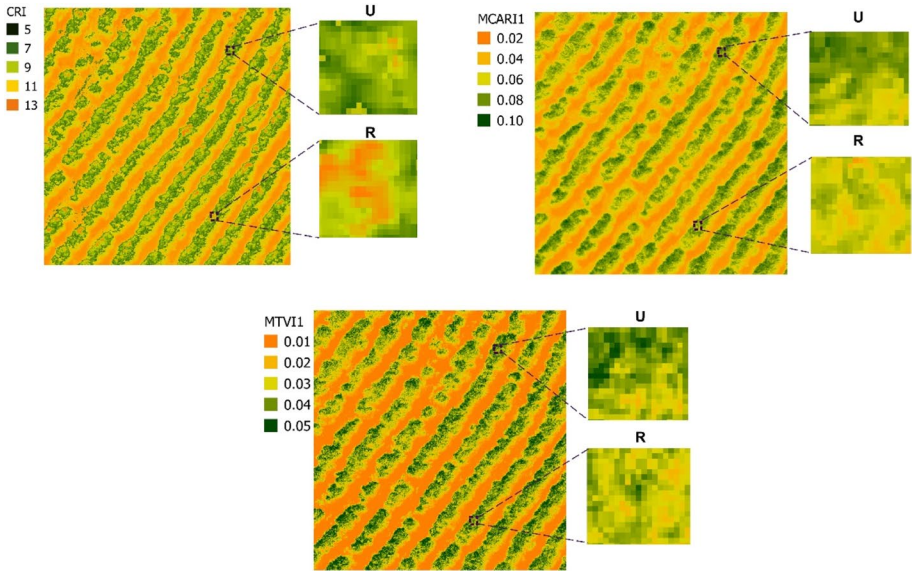

Fig. 8 Representation of the CRI, MCARI1, and MTVI1 vegetation indices for plants with unripe (G) and ripe (R) coffee fruits

nitrogen demand as demonstrated by Reis et al. (2015). Moreover, the temporal change of fruit color caused by the reduction of chlorophyll and accumulation of anthocyanins might have influenced the crop spectral response as well (Castro & Marraccini, 2006).

Overall, the results obtained in this study reveals the great potential of using RS in the coffee crop for fruit ripeness monitoring. A recommendation for future studies would be the use of VIs combined with plant characteristics (e.g., canopy volume and yield), and machine learning algorithms to predict the fruit ripeness and develop pre-harvest maps. These maps can be used as decision support tools for monitoring and identifying on a temporal scale those plants ready and not ready for harvest throughout the end of the season. In addition, future studies should include the acquisition of data from multiple seasons and several commercial fields to validate the methodology.

Conclusions

A UAV-based modified multispectral camera was used for coffee ripeness monitoring in five fields with distinct characteristics. Laboratory pre-tests showed an overlap between the red and NIR bands of the camera, in which reflectance registered in the red band corresponded to 86.6% of the NIR reflectance. Despite that, the camera showed potential for temporal monitoring of the coffee crop. Among the vegetation indices (VIs) evaluated, the CRI, MCARI1, and MTVI1 presented the highest sensitivity when discriminating plants with unripe fruits from those with ripe fruits in most fields. However, the performance of these VIs was directly influenced by the crop yield and canopy volume.

Acknowledgements This study was partially financed by the Coordenação de Aperfeiçoamento de Pessoal de Nível Superior (CAPES, Coordination for the Improvement of Higher Education Personnel)—Finance

Code 001, by the Fundação de Apoio à Pesquisa do Estado de Minas Gerais (FAPEMIG, Research Support Foundation of the State of Minas Gerais, Brazil) and by the Conselho Nacional de Desenvolvimento Científico e Tecnológico (CNPq, The Brazilian National Council for Scientific and Technological Development).

Author contributions Funding acquisition, FdAdCP and DMdQ; Investigation, JTFR; Methodology, JTFR; Project administration, FdAdCP; Resources, FdAdCP and DMdQ; Supervision, FdAdCP, DMdQ and FMdMV; Writing—original draft, JTFR and RNM; Writing—review & editing, JTFR, FdAdCP, DMdQ, FMdMV, DSMV and RNM. All authors have read and agreed to the published version of the manuscript.

Declarations

Conflict of interest The authors declare that they have no conflict of interest.

References

Amaral, J. A. T., Da Matta, F. M., & Rena, A. B. (2001). Effects of fruiting on the growth of arabica coffee trees as related to carbohydrate and nitrogen status and to nitrate reductase activity. *Revista Brasileira de Fisiologia Vegetal, 13*(1), 66–74. https://doi.org/10.1590/S0103-31312001000100008

Aparecido, L. E. de O., Rolim, G. de S., DeMoraes, J. R. da S. C., Valeriano, T. T. B., & Lense, G. H. E. (2018). Maturation periods for *Coffea arabica* cultivars and their implications for yield and quality in Brazil. *Journal of the Science of Food and Agriculture, 98*(10), 3880–3891. https://doi.org/10.1002/jsfa.8905

Baret, F., & Guyot, G. (1991). Potentials and limits of vegetation indices for LAI and APAR assessment. *Remote Sensing of Environment, 35*, 161–173.

Bernardes, T., Moreira, M. A., Adami, M., Giarolla, A., & Rudorff, B. F. T. (2012). Monitoring biennial bearing effect on coffee yield using MODIS remote sensing imagery. *Remote Sensing, 4*(9), 2492–2509. https://doi.org/10.3390/rs4092492

De Castro, R. D., & Marraccini, P. (2006). Cytology, biochemistry and molecular changes during coffee fruit development. *Brazilian Journal of Plant Physiology, 18*(1), 175–199.

Coburn, C. A., Smith, A. M., Logie, G. S., & Kennedy, P. (2018). Radiometric and spectral comparison of inexpensive camera systems used for remote sensing. *International Journal of Remote Sensing, 39*(15–16), 4869–4890. https://doi.org/10.1080/01431161.2018.1466085

Corti, M., Cavalli, D., Cabassi, G., Vigoni, A., Degano, L., & Marino Gallina, P. (2019). Application of a low-cost camera on a UAV to estimate maize nitrogen-related variables. *Precision Agriculture, 20*(4), 675–696. https://doi.org/10.1007/s11119-018-9609-y

Del Pozo, S., Rodríguez-Gonzálvez, P., Hernández-López, D., & Felipe-García, B. (2014). Vicarious radiometric calibration of a multispectral camera on board an unmanned aerial system. *Remote Sensing, 6*(3), 1918–1937. https://doi.org/10.3390/rs6031918

Fagan, E. B., de Souza, C. H. E., Pereira, N. M. B., & Machado, V. J. (2011). Effect of time on coffee bean (Coffea sp.) growth in cup quality. *Bioscience Journal, 27*(5), 729–738.

Favarin, J. L., Dourado Neto, D., García y García, A., Villa Nova, N. A., & Favarin, M. da G. G. V. (2002). Equações para a estimativa do índice de área foliar do cafeeiro. *Pesquisa Agropecuária Brasileira, 37*(6), 769–773. https://doi.org/10.1590/S0100-204X2002000600005

Furfaro, R., Ganapol, B. D., Johnson, L. F., & Herwitz, S. R. (2007). Neural network algorithm for coffee ripeness evaluation using airborne images. *Applied Engineering in Agriculture, 23*(3), 379–387.

Gitelson, A. A., Kaufman, Y. J., & Merzlyak, M. N. (1996). Use of a green channel in remote sensing of global vegetation from EOS-MODIS. *Remote Sensing of Environment, 58*(3), 289–298. https://doi.org/10.1016/S0034-4257(96)00072-7

GitHub-OpenDroneMap/ODM. (n.d.). https://github.com/OpenDroneMap/ODM/. Accessed 15 May 2019.

GitHub-OpenDroneMap/WebODM. (n.d.). https://github.com/OpenDroneMap/WebODM. Accessed 18 August 2019.

Guimarães, E. R., Leme, P. H. M. V., De Rezende, D. C., Pereira, S. P., & Dos Santos, A. C. (2019). The brand new Brazilian specialty coffee market. *Journal of Food Products Marketing, 25*(1), 49–71. https://doi.org/10.1080/10454446.2018.1478757

Haboudane, D., Miller, J. R., Pattey, E., Zarco-Tejada, P. J., & Strachan, I. B. (2004). Hyperspectral vegetation indices and novel algorithms for predicting green LAI of crop canopies: Modeling and

validation in the context of precision agriculture. *Remote Sensing of Environment, 90*(3), 337–352. https://doi.org/10.1016/j.rse.2003.12.013

Hall, F. G., Strebel, D. E., Nickeson, J. E., & Goetz, S. J. (1991). Radiometric rectification: Toward a common radiometric response among multidate, multisensor images. *Remote Sensing of Environment, 35*, 11–27.

Herwitz, S. R., Johnson, L. F., Dunagan, S. E., Higgins, R. G., Sullivan, D. V., Zheng, J., et al. (2004). Imaging from an unmanned aerial vehicle: Agricultural surveillance and decision support. *Computers and Electronics in Agriculture, 44*(1), 49–61. https://doi.org/10.1016/j.compag.2004.02.006

Hruska, R., Mitchell, J., Anderson, M., & Glenn, N. F. (2012). Radiometric and geometric analysis of hyperspectral imagery acquired from an unmanned aerial vehicle. *Remote Sensing, 4*(9), 2736–2752. https://doi.org/10.3390/rs4092736

Huang, S., Miao, Y., Zhao, G., Yuan, F., Ma, X., Tan, C., Yu, W., Gnyp, M. L., Lenz-Wiedemann, V. I. S., Rascher, U., & Bareth, G. (2015). Satellite remote sensing-based in-season diagnosis of rice nitrogen status in Northeast China. *Remote Sensing, 7*(8), 10646–10667. https://doi.org/10.3390/rs70810646

Iqbal, F., Lucieer, A., & Barry, K. (2018). Simplified radiometric calibration for UAS-mounted multispectral sensor. *European Journal of Remote Sensing, 51*(1), 301–313. https://doi.org/10.1080/22797254.2018.1432293

Johnson, L. F., Herwitz, S. R., Lobitz, B. M., & Dunagan, S. E. (2004). Feasibility of monitoring coffee field ripeness with airborne multispectral imagery. *Applied Engineering in Agriculture, 20*(6), 845–849.

Jordan, C. F. (1969). Derivation of leaf-area index from quality of light on the forest floor. *Wiley on Behalf of the Ecological Society of America Stable, 50*(4), 663–666.

Laviola, B. G., Martinez, H. E. P., de Souza, R. B., Salomão, L. C. C., & Cruz, C. D. (2009). Macronutrient accumulation in coffee fruits at Brazilian zona da mata conditions. *Journal of Plant Nutrition, 32*(6), 980–995. https://doi.org/10.1080/01904160902872164

Lebourgeois, V., Bégué, A., Labbé, S., Mallavan, B., Prévot, L., & Roux, B. (2008). Can commercial digital cameras be used as multispectral sensors? A crop monitoring test. *Sensors, 8*(11), 7300–7322. https://doi.org/10.3390/s8117300

Lelong, C. C. D., Burger, P., Jubelin, G., Roux, B., Labbé, S., & Baret, F. (2008). Assessment of unmanned aerial vehicles imagery for quantitative monitoring of wheat crop in small plots. *Sensors, 8*(5), 3557–3585. https://doi.org/10.3390/s8053557

Logie, G. S. J., & Coburn, C. A. (2018). An investigation of the spectral and radiometric characteristics of low-cost digital cameras for use in UAV remote sensing. *International Journal of Remote Sensing, 39*(15–16), 4891–4909. https://doi.org/10.1080/01431161.2018.1488297

Lu, B., & He, Y. (2017). Species classification using Unmanned Aerial Vehicle (UAV)-acquired high spatial resolution imagery in a heterogeneous grassland. *ISPRS Journal of Photogrammetry and Remote Sensing, 128*, 73–85. https://doi.org/10.1016/j.isprsjprs.2017.03.011

Lulé, T., Benthien, S., Keller, H., Muütze, F., Rieve, P., Seibel, K., Sommer, M., & Bohm, M. (2000). Sensitivity of CMOS based imagers and scaling perspectives. *IEEE Transactions on Electron Devices, 47*(11), 2110–2122. https://doi.org/10.1109/16.877173

Marin, D. B., Alves, M. de C., Pozza, E. A., Belan, L. L., & Freitas, M. L. de O. (2019). Multispectral radiometric monitoring of bacterial blight of coffee. *Precision Agriculture, 20*(5), 959–982. https://doi.org/10.1007/s11119-018-09623-9

Nijland, W., Jong, R. D., De Jong, S. M., Wulder, M. A., Bater, C. W., & Coops, N. C. (2014). Agricultural and Forest Meteorology Monitoring plant condition and phenology using infrared sensitive consumer grade digital cameras. *Agricultural and Forest Meteorology, 184*, 98–106. https://doi.org/10.1016/j.agrformet.2013.09.007

Nogueira Martins, R., Pinto, F. de A. de C., Queiroz, D. M. de, Valente, D. S. M., & Rosas, J. T. F. (2021). A novel vegetation index for coffee ripeness monitoring using aerial imagery. *Remote Sensing, 13*(2), 1–16. https://doi.org/10.3390/rs13020263

Nogueira, S. M. C., Moreira, M. A., & Volpato, M. M. L. (2018). Relationship between coffee crop productivity and vegetation indexes derived from oli/landsat-8 sensor data with and without topographic correction. *Engenharia Agricola*. https://doi.org/10.1590/1809-4430-Eng.Agric.v38n3p387-394/2018

Parreiras, T. C., Lense, G. H. E., Moreira, R. S., Santana, D. B., & Mincato, R. L. (2020). Using unmanned aerial vehicle and machine learning algorithm to monitor leaf nitrogen in coffee. *Coffee Science, 15*(1), 1–9. https://doi.org/10.25186/.v15i.1736

Paseto, L., & Patino, M. T. O. (2019). Recognition of key drivers to the improvement of competitiveness strategies in Brazilian Coffee. *International Journal of Advanced Engineering Research and Science, 6*(7), 188–196. https://doi.org/10.22161/ijaers.6723

Pimenta, C. J., Angélico, C. L., & Chalfoun, S. M. (2018). Challengs in coffee quality: Cultural, chemical and microbiological aspects. *Ciencia e Agrotecnologia, 42*(4), 337–349. https://doi.org/10.1590/1413-70542018424000118

Putra, B. T. W., & Soni, P. (2017). Evaluating NIR-Red and NIR-Red edge external filters with digital cameras for assessing vegetation indices under different illumination. *Infrared Physics and Technology, 81*, 148–156. https://doi.org/10.1016/j.infrared.2017.01.007

QGIS Development Team. (2016). QGIS Geographic Information System. *Open Source Geospatial Foundation Project*. http://qgis.osgeo.org

R Core Team. (2019). R: A language and environment for statistical computing. Vienna, Austria. http://www.r-project.org

Rabatel, G., Gorretta, N., & Labbé, S. (2014). Getting simultaneous red and near-infrared band data from a single digital camera for plant monitoring applications: Theoretical and practical study. *Biosystems Engineering, 117*(1), 2–14. https://doi.org/10.1016/j.biosystemseng.2013.06.008

Ramirez, G. M., & Zullo Júnior, J. (2010). Estimation of biophysical parameters of coffee fields based on high-resolution satellite images. *Engenharia Agrícola, 30*(3), 468–479.

Reis, A. R., Favarin, J. L., Gratão, P. L., Capaldi, F. R., & Azevedo, R. A. (2015). Antioxidant metabolism in coffee (*Coffea arabica* L.) plants in response to nitrogen supply. *Theoretical and Experimental Plant Physiology, 27*, 203–213. https://doi.org/10.1007/s40626-015-0045-3

Rosas, J. T. F., de Carvalho Pinto, F. de A., Queiroz, D. M. de, de Melo Villar, F. M., Martins, R. N., & Silva, S. de A. (2020). Low-cost system for radiometric calibration of UAV-based multispectral imagery. *Journal of Spatial Science*. https://doi.org/10.1080/14498596.2020.1860146

Rouse, J. W., Haas, R. H., Schell, J. A., Deering, D. W., & Freden, S. C. (1973). Monitoring vegetation systems in the Great Plains with ERTS. In *Proceedings of 3rd Earth Resources Technology Satellite-1 Symposium* (pp. 309–317). Washington.

Santos, L. M., Ferraz, G. A. e. S., Barbosa, B. D. de S., Diotto, A. V., Maciel, D. T., & Xavier, L. A. G. (2020). Biophysical parameters of coffee crop estimated by UAV RGB images. *Precision Agriculture, 21*(6), 1227–1241. https://doi.org/10.1007/s11119-020-09716-4

Senthilnath, J., Dokania, A., Kandukuri, M., Ramesh, K. N., Anand, G., & Omkar, S. N. (2016). Detection of tomatoes using spectral-spatial methods in remotely sensed RGB images captured by UAV. *Biosystems Engineering, 146*, 16–32. https://doi.org/10.1016/j.biosystemseng.2015.12.003

Simões, R. D. O., Faroni, L. R. D., & Queiroz, D. M. de. (2008). Qualidade dos grãos de café (*Coffea arábica* l.) Em coco processados por via seca. *Revista caatinga, 21*(2), 139–146.

Sonobe, R., & Wang, Q. (2017). Hyperspectral indices for quantifying leaf chlorophyll concentrations performed differently with different leaf types in deciduous forests. *Ecological Informatics, 37*, 1–9. https://doi.org/10.1016/j.ecoinf.2016.11.007

Tucker, C. J. (1979). Red and photographic infrared linear combinations for monitoring vegetation. *Remote Sensing of Environment, 8*(2), 127–150. https://doi.org/10.1016/0034-4257(79)90013-0

Valente, J., Almeida, R., & Kooistra, L. (2019). A comprehensive study of the potential application of flying ethylene-sensitive sensors for ripeness detection in apple orchards. *Sensors (Switzerland), 19*(2), 372. https://doi.org/10.3390/s19020372

Varão, T., Marcondes, D., Pereira, B., Anchieta, J., & Neto, G. (2019). Prediction of black, immature and sour defective beans in coffee blends by using Laser-Induced Breakdown Spectroscopy. *Food Chemistry, 278*(November 2018), 223–227. https://doi.org/10.1016/j.foodchem.2018.11.062

Vincini, M., Frazzi, E., & D'Alessio, P. (2007). Narrow-band vegetation indexes from hyperion and directional CHRIS/PROBA data for canopy chlorophyll density estimation in maize. In *Proceedings of the Envisat Symposium* (pp. 23–27). Montreux, Switzerland.

Volsi, B., Telles, T. S., Caldarelli, C. E., & Camara, M. R. G. da. (2019). The dynamics of coffee production in Brazil. *PLoS One, 14*(7), e0219742. https://doi.org/10.1371/journal.pone.0219742

Wang, C., & Myint, S. W. (2015). A simplified empirical line method of radiometric calibration for small unmanned aircraft systems-based remote sensing. *IEEE Journal of Selected Topics in Applied Earth Observations and Remote Sensing, 8*(5), 1876–1885. https://doi.org/10.1109/JSTARS.2015.2422716

Yu, N., Li, L., Schmitz, N., Tian, L. F., Greenberg, J. A., & Diers, B. W. (2016). Development of methods to improve soybean yield estimation and predict plant maturity with an unmanned aerial vehicle based platform. *Remote Sensing of Environment, 187*, 91–101. https://doi.org/10.1016/j.rse.2016.10.005

Zhang, C., & Kovacs, J. M. (2012). The application of small unmanned aerial systems for precision agriculture: A review. *Precision Agriculture, 13*(6), 693–712. https://doi.org/10.1007/s11119-012-9274-5

Publisher's Note Springer Nature remains neutral with regard to jurisdictional claims in published maps and institutional affiliations.